

## Article

# Characterizing Aqueous Cd<sup>2+</sup> Removal by Plant Biochars from Qinghai–Tibet Plateau

Wenxuan Li <sup>1,2,\*</sup>, Xueli Wang <sup>1,2</sup>, Haizhen Kong <sup>3</sup> and Dan Zhang <sup>1,2</sup><sup>1</sup> School of Water and Environment, Chang'an University, Xi'an 710054, China<sup>2</sup> Key Laboratory of Subsurface Hydrology and Ecological Effects in Arid Region of Ministry of Education, Chang'an University, Xi'an 710054, China<sup>3</sup> Basic Teaching Department, Handan Vocational College of Science and Technology, Handan 056005, China

\* Correspondence: wenxuanli@chd.edu.cn

**Abstract:** Increased anthropogenic activities have caused cadmium pollution in Qinghai–Tibet Plateau, which is harmful to human health. This paper investigated aqueous Cd<sup>2+</sup> adsorption using biochar of three typical vegetation types in cold and arid areas of the Qinghai–Tibet Plateau: (i) Chinese wolfberry (GBB), (ii) highland barley (QBB), and (iii) seabuckthorn (SBB). In order to investigate the effect of pyrolysis temperature on the performance of biochar for cadmium adsorption, three types of biochar were prepared at 350 °C, 500 °C, and 650 °C. The as-prepared biochar was characterized by scanning electron microscopy (SEM), Thermogravimetric (TG), Fourier transform infrared spectroscopy (FT-IR), and Brauer–Emmett–Teller (BET) analysis. The results showed that the biochar prepared at 650 °C had the best adsorption capacity. Compared with QBB and SBB, the GBB had a higher Cd<sup>2+</sup> adsorption capacity of 19.48 mg/g. Moreover, the effects of biochar dosage, experimental temperature, and biochar preparation temperature on the adsorption of Cd<sup>2+</sup> by biochar and the interaction between the factors were investigated using Box–Behnken Design (BBD). As a result, the amount of biochar dosage showed the most obvious influence on Cd<sup>2+</sup> adsorption capacity, followed by sample preparation temperature and experimental adsorption temperature. This study paves the way for the design of biochar for Cd<sup>2+</sup> adsorption in wastewater.

**Keywords:** biochar; adsorption; response surface methodology; heavy metal cadmium

**Citation:** Li, W.; Wang, X.; Kong, H.; Zhang, D. Characterizing Aqueous Cd<sup>2+</sup> Removal by Plant Biochars from Qinghai–Tibet Plateau. *Water* **2022**, *14*, 4085. <https://doi.org/10.3390/w14244085>

## Academic Editors:

Chicgoua Noubactep, Cuijie Feng, Qian Sun and Qizhao Wang

Received: 8 November 2022

Accepted: 7 December 2022

Published: 14 December 2022

**Publisher's Note:** MDPI stays neutral with regard to jurisdictional claims in published maps and institutional affiliations.



**Copyright:** © 2022 by the authors. Licensee MDPI, Basel, Switzerland. This article is an open access article distributed under the terms and conditions of the Creative Commons Attribution (CC BY) license (<https://creativecommons.org/licenses/by/4.0/>).

## 1. Introduction

Over the past 40 years of reform and opening up, Chinese society has developed rapidly in all aspects [1]. However, due to the rapid development of industry, the emission of pollutants in metal mining, metallurgy, papermaking and other industries [2], automobile exhaust, excessive use of pesticides and fertilizers and other factors have caused heavy metal pollution of surface water [3,4]. Known as the “third pole” and the “roof of the world,” the Qinghai–Tibet Plateau, which has the highest average altitude in the world and many unique environments, is one of the regions least affected by human activities [5]. Under natural conditions, relatively low heavy metal element content in the Qinghai–Tibet plateau surface water [6], but in recent years, along with the atmospheric precipitation, mining, and agricultural production, such as the impact of human activities, the Qinghai–Tibet plateau ecological environment gradually affected, mainly from the plateau of heavy metals pollution of surface water and pesticide chemical fertilizer, crop production in the process of mining, etc. [7,8]. According to the statistics of several regions, the heavy metal content in the surface water of the Qinghai–Tibet Plateau is generally at a low level, but the pollution is becoming more and more serious, and sufficient attention should be paid to it [9]. Among many pollution elements, Cd<sup>2+</sup> is a highly toxic heavy metal, which has been listed as a human carcinogen by the International Agency for Research on Cancer (IARC) and has great harm to kidneys, prostate, pancreas, lungs, and bone [10,11]. Therefore, it is

of great significance to conduct in-depth research on the behavior characteristics of organic matter in the process of cadmium migration [12].

Biochar is an insoluble and stable highly aromatic carbon-rich solid material produced by the pyrolysis of biomass materials (crop straw, wood, animal manure, sludge, wood chips, etc.) under fully or partially anoxic conditions and at a certain temperature [13,14]. Many researchers have shown that biochar has a unique pore structure, a large specific surface area, and carries a large number of negative charges and abundant functional groups on its surface, which makes it have good adsorption capacity [15] and can be applied as a new type of passivating agent in soil environmental pollution remediation. The performances, such as surface properties and pore structure of biochar prepared from different raw materials, vary widely, affecting biochar's adsorption activity [16,17]. Xu et al. investigated the adsorption of methyl violet by biochar from four crop straws. They found that their adsorption capacity varied with their feedstocks in the following order [18]. Xu et al. reported that cow dung biochar was more effective than rice husk biochar in the removal of Pb, Cu, Zn, and Cd from mono and polymetallic solutions [19]. Bernardo et al. studied co-pyrolysis biochar of pine wood, old tires, and plastic waste for Pb removal from aqueous media. However, they concluded that mixed pyrolysis of the three feedstocks did not improve the removal efficiency of the resulting char for Pb [20].

In addition, the factors affecting the adsorption of heavy metals by biochar include pyrolysis temperature, test temperature, and biochar content [21]. Cao et al. used cow dung to prepare biochar and found that the adsorption of Pb by biochar prepared at 200 °C was significantly higher than that by biochar prepared at 350 °C [22,23]. Liu et al. investigated the Pb adsorption characteristics of pine and straw biochar at solution temperatures of 25, 35, and 45 °C. The results showed that the adsorption rate of Pb on biochar was faster at higher solution temperatures than at lower temperatures [24]. Since the biochar type, preparation conditions, and experimental factors can affect the final adsorption of heavy metals [25], in the past, most studies have selected the optimal biochar, preparation conditions, and experimental factors in a trial-and-error manner by adsorption capacity in static conditions experiments [26], this method is experimental, unpredictable, and, most importantly, do not consider the interactions between the three factors affecting the adsorption capacity during the adsorption of heavy metals on biochar; therefore, it is urgent to find an accurate, simple, and predictive method. Response surface methodology (RSM) [27,28] is a statistical experimental design for optimizing biological processes, also known as regression design, and this type of experimental design problem requires finding quantitative patterns between the experimental indicators and the factors. Regression design is an experimental design method that synthesizes results through several disciplines, including statistics, mathematics, and computer science, and it has been successfully applied to optimize bio-engineering and food engineering because it takes into account many factors and has very tedious operations that are inferior to those of manual operations [29,30].

In this study, three typical plateau plants of Chinese wolfberry (GBB), highland barley (QBB) and seabuckthorn (SBB) were used as raw materials for the preparation of biochar by pyrolysis at different temperatures. The adsorption capacity of three types of biochar for cadmium was investigated using surface response analysis and explored the feasibility of parameter optimization for heavy metal adsorption on biochar using the surface response method in anticipation of providing theoretical guidance for the application of vegetated biochar in cold and arid plateau areas for the treatment of heavy metal polluted wastewater.

## 2. Materials and Methods

In this experiment, barley, wolfberry, and sea buckthorn straws from eastern Qinghai, China. were used as raw materials. Firstly, the three kinds of straw were cleaned, crushed by a Chinese medicine crusher, dried at 105 °C, and then prepared the straw biochar by oxygen-limited temperature control carbonization method. The prepared plant powder was then subjected to limited oxygen pyrolysis in a muffle furnace. The temperatures were controlled at 350 °C, 500 °C, and 650 °C and ramped up to the target temperature at a

rate of 20 °C/min and then held for 2 h. Cool naturally to room temperature, take out and grind, pass 100 mesh sieve and seal up for later use. The obtained barley biochar was labeled as QBB350, QBB500, and QBB650 according to different preparation temperatures.

### 2.1. Characterization Analysis

The C, H, and N contents of biological carbon were determined by an elemental analyzer (Vario ELcube, Hanau, Germany), and the O content was calculated by the mass balance method. PH was measured with a DELTA 320 pH meter (MettlerToledo, Zurich, Switzerland). FEI Quanta 650 (FEI, Waltham, MA, USA) scanning electron microscope was used to observe biochar's microstructure and morphology characteristics. The changes of functional groups on the surface of biochar were tested, and FT-IR profiles were obtained using FT-IR-1500 (GLFore, Suzhou, China) Fourier transform infrared spectrometer and potassium bromide pressure test method. The parameters such as specific surface, pore type, and pore volume of the experimentally prepared biochar were determined using a fully automatic specific surface area and porosity analyzer Gemini V2380 (Micromeritics Instrument Co., Norcross, GA, USA). The TGA Q600 SDT (TA, Newcastle, DE, USA) thermogravimetric analyzer was used to measure (Differential scanning calorimetry (DSC) and Thermogravimetric analysis (TGA) under an N<sub>2</sub> atmosphere and generate the TG (Thermogravimetric Analysis)-DTG (Derivative thermogravimetry)- Differential thermal analysis (DTA) curve.

### 2.2. Experimental Method of RSM

In this study, a Box–Behnken Design (BBD) with N = 3 was selected. The dosage of biochar (X1), experimental temperature (X2), and preparation temperature of biochar (X3) were taken as three independent variables. Three levels were taken for each factor, and the adsorption amount of cadmium ion (set as Y) was taken as the response value. The influence of three factors on the response value and the correlation among variables were investigated, and the adsorption parameters of cadmium ions were optimized. Different types of biochar with different preparation temperatures were accurately weighed into 50 mL conical flasks, and 20 mL of Cd<sup>2+</sup> solution with a concentration of 100 mg/L was added to make the final dosage of biochar 0.1 g/L, 0.3 g/L, and 0.5 g/L, respectively. The initial pH of all solutions was adjusted to 7.0. Moreover, the solution was placed in a 100 r/min thermostatic oscillator at 25 °C, 35 °C, and 45 °C for a certain period, then the concentration of Cd<sup>2+</sup> in the filtrate was determined by ICP-MS (Thermo Fisher, Waltham, MA, USA) (Inductively coupled plasma emission spectrometer) through a 0.45 µm filter membrane. All adsorption experiments were performed three times to ensure the reproducibility of the data. Moreover, all the above experiments were performed simultaneously with blank experiments. The effect caused by the loss of the bottle wall and other samples is negligible. The samples were taken at 0.5 h intervals with constant temperature shaking for 180 min. The adsorption capacity of Cadmium ion at time t Q<sub>t</sub> (mg/kg) is calculated by the following formula:

$$Q_t = \frac{V \times (C_0 - C_t)}{m} \quad (1)$$

where V (mL) is the volume of solution; C<sub>0</sub> (mg/L) is the initial concentration of cadmium ion, C<sub>t</sub> (mg/L) is the concentration at time t, and m (kg) is the sample mass.

Preliminary experimental data and graphs were analyzed by Origin 2018 (<https://www.originlab.com/origin>, accessed on 6 December 2022). Design Expert 8.0.6 software (<https://www.statease.com/software/design-expert/>, accessed on 6 December 2022) was used to optimize the scheme Design and analyze the experimental results of the mixed experiment of biochar dosage + preparation temperature + experiment temperature.

### 2.3. Adsorption Kinetics Test

About 0.1 g of all biochar samples were accurately weighed and placed in a 50 mL corkscrew conical flask. A series of 20 mL 100 mg/L Cd<sup>2+</sup> solutions were added respectively,

and the  $\text{Cd}^{2+}$  solutions were prepared with 0.01 mol/L  $\text{NaNO}_3$  background solution at 25 °C (298 K, pH = 7.0), oscillating at 120 r/min for 30 min, 60 min, 90 min, 120 min, 150 min, and 180 min, respectively, in a constant temperature oscillator. Three parallel samples were taken at each time, and no samples were added for a blank experiment. The effect caused by the wall and other losses is negligible. After the oscillation, the samples were filtered through a 0.45  $\mu\text{m}$  aqueous phase filtration membrane. The concentration of  $\text{Cd}^{2+}$  in the filtrate was determined by ICP-MS (Thermo Fisher, Waltham, MA, USA) type inductively coupled plasma emission spectrometer (In this study,  $\text{Cd}^{2+}$  solution was configured with  $\text{Cd}(\text{NO}_3)_2 \cdot 4\text{H}_2\text{O}$ . All reagents are pure analytical grade, purchased from Shanghai Aladdin Biochemical Technology Co., LTD., Shanghai, China).

### 3. Results and Discussion

#### 3.1. Characterization Analysis

Table 1 shows the elemental composition, ash content, and yield of biochar prepared at different temperatures. The productivity of QBB is the lowest at different temperatures, which is because hemicellulose and cellulose contained in QBB are easily and completely decomposed at about 350 °C. SBB and GBB have relatively high lignin content and need a higher temperature than cellulose to decompose; while the yield of the same biochar decreased as the preparation temperature increased, the ash content increased, probably because ash, as an inorganic component, broke some chemical bonds and released CO and other gases, resulting in a large amount of carbon-containing substances that caused the ash content to increase. In addition, as the preparation temperature of the same biochar increased, the proportion of N, H, and O gradually decreased while the content of C gradually increased, which was because many carbon-rich substances needed to consume large amounts of oxygen to be produced as the temperature continued to increase and the pyrolysis reaction continued. The value of H/C also decreased as the preparation temperature increased, which showed that the higher the preparation temperature, the more fully the biochar was carbonized, the dehydration reaction occurred, and the aromaticity was higher. On the contrary, the polarity of biochar decreases with increasing preparation temperature.

**Table 1.** Elemental composition, ash content, and yield of biochar prepared at different temperatures.

Sample Name	Productivity (%)	Ash Content (%)	C (%)	H (%)	O (%)	H/C	(N + O)/C	O/C
GBB350	35.2	6.31	71.54	3.97	21.65	0.72	0.37	0.15
GBB500	28.9	11.7	74.15	2.81	12.11	0.44	0.33	0.06
GBB650	25.1	19.65	74.42	1.62	11.79	0.16	0.28	0.06
QBB350	29.4	10.56	64.33	2.98	27.43	0.41	0.31	0.11
QBB500	21.2	19.64	69.78	2.54	18.97	0.28	0.34	0.10
QBB650	16.3	26.16	70.76	1.88	10.76	0.27	0.24	0.03
SBB350	43.2	4.51	74.18	3.79	19.22	0.56	0.41	0.22
SBB500	35.5	9.82	81.67	1.76	10.65	0.21	0.33	0.15
SBB650	30.3	13.22	87.15	2.91	6.31	0.11	0.25	0.08

#### 3.2. Electron Microscopic Analysis

SEM was used to analyze the microstructure and morphology characteristics of the three biochar, as shown in Figure 1. Among the three types of biochar, it can be seen in Figure 1c that GBB has the most developed pore structure due to its high lignin and organic matter content and sufficient volatilization during the pyrolysis process, with good tubular pore connectivity and many more tiny pores formed on the tube wall, which is the best adsorption condition among the three types of biochar, followed by QBB, as can be seen in Figure 1a, although QBB does not develop smaller. The worst adsorption condition is SBB, and it can be seen in Figure 1b that due to the extremely irregular development of its tubular pores, many of its internal pores become dead pores, and the adsorbed substances

cannot enter these pores for adsorption, although SBB has a larger bulk structure than other biochars, the pore space for adsorption is smaller than that of the other two biochars.

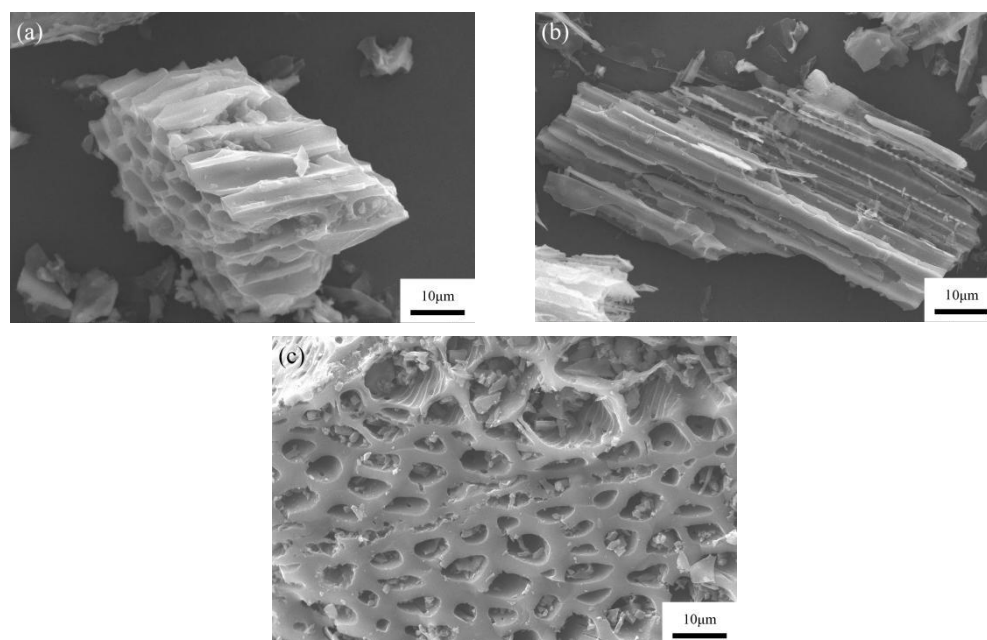


**Figure 1.** The SEM images of (a) QBB, (b) SBB, and (c) GBB at preparation temperature  $T = 650\text{ }^{\circ}\text{C}$ .

It can be seen visually in Figure 2 that the more effective pores of biochar, the better the connectivity and the larger the space available for adsorption, and the smaller the pores, the larger the specific surface area and the stronger the adsorption capacity.

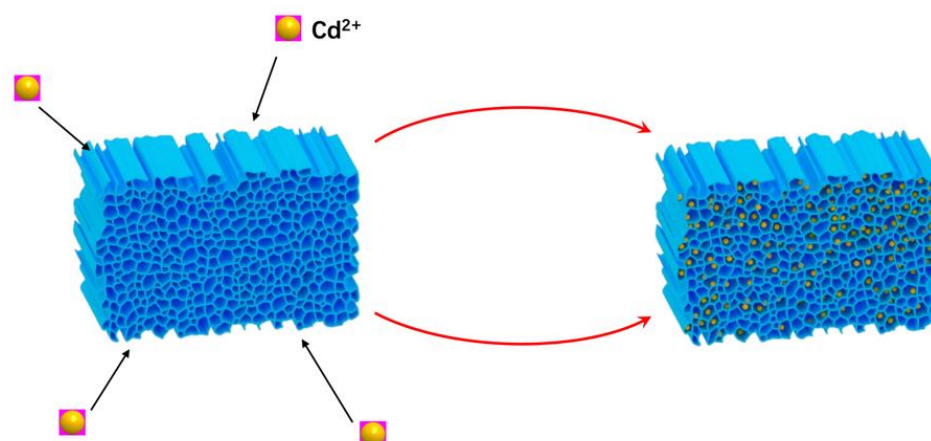


**Figure 2.** Schematic diagram of the possibility of the superiority of GBB adsorption.

### 3.3. Analysis of Adsorption Kinetics

Figure 3 shows the experimental results of the adsorption kinetics of three biochar at different preparation temperatures. It can be seen that the adsorption curves of biochar prepared by the three raw materials at  $350\text{ }^{\circ}\text{C}$  are relatively flat, and there is a big gap between the adsorption curves of biochar prepared at the other two temperatures. The saturated adsorption capacity of biochar prepared at this temperature is very small. The adsorption curve of biochar prepared at a higher temperature is more curved and fluctuated, and the biochar prepared by the three raw materials has a greater adsorption capacity at each time of the adsorption process [31]. This indicates that the adsorption capacity

of biochar increases with the increase of the preparation temperature of biochar, and the preparation temperature has a significant effect on the adsorption capacity of biochar.

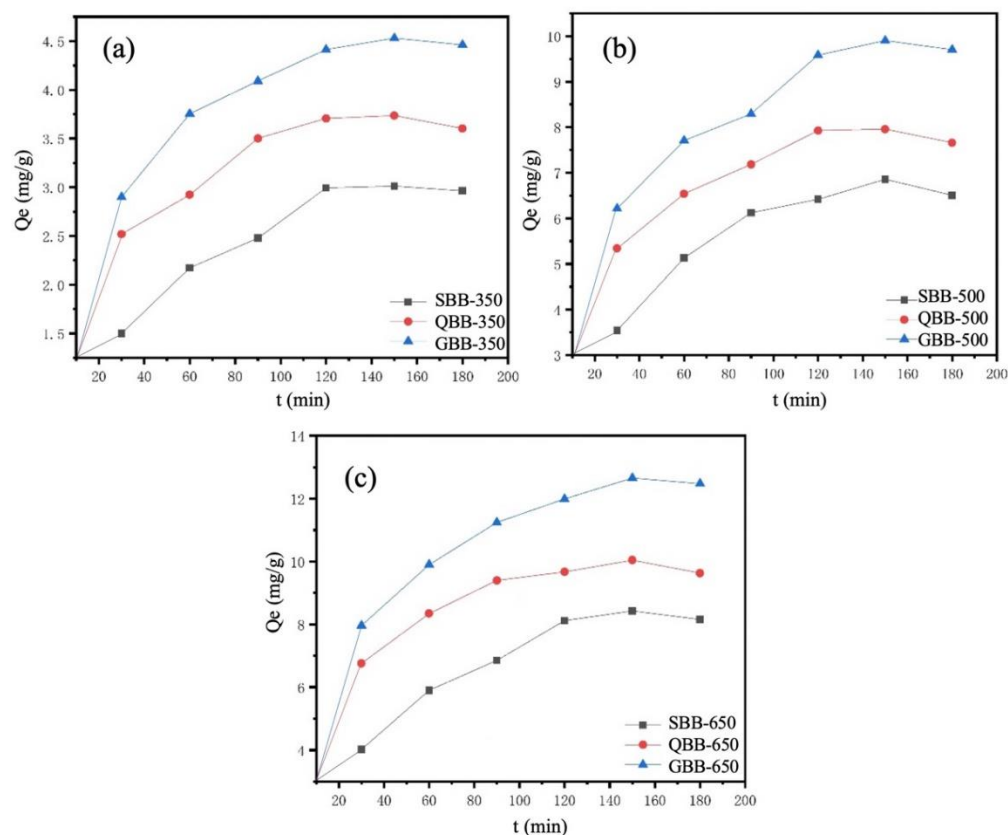


**Figure 3.** Experimental results of adsorption kinetics of three biochar at different preparation temperatures: (a) Cd<sup>2+</sup> adsorption curves of GBB, QBB, and SBB at 350 °C; (b) Cd<sup>2+</sup> adsorption curves of GBB, QBB, and SBB at 500 °C; (c) Adsorption curves of Cd<sup>2+</sup> at 650 °C for GBB, QBB, and SBB.

As can be seen from Figure 3a–c, at three preparation temperatures, the adsorption capacity follows the rule of GBB > QBB > SBB. Moreover, the time to reach the saturated adsorption capacity is the same, at about 120 min, which means that the biochar with a larger adsorption capacity has a faster absorption rate; that is, among the three biochar, GBB biochar has the best adsorption performance, QBB biochar comes second, and SBB biochar is the worst.

Combined with the preparation temperature and raw materials, the adsorption performance of GBB650 is the best.

### 3.4. Infrared Analysis

The infrared spectra of GBB at different temperatures are analyzed in Figure 4, and it can be seen that the types of functional groups contained in biochar prepared from the same biomass feedstock at different temperatures are unchanged. However, the absorption peak representing hydroxyl-OH slowed down as the preparation temperature increased, which indicated that the number of hydroxyl groups decreased as the preparation temperature increased. As the pyrolysis temperature increases, the loss of oxygen-containing functional groups results from dehydration, decarbonylation reactions, and decarboxylation reactions leading to the growth of the aromatic structure. At the same time, absorption peaks representing C=C and C-C bonds increased with the increase in preparation temperature, indicating that the number of these two chemical bonds increased, and the aromatics and stability of biochar increased with the increase of preparation temperature, which was consistent with the results of elemental composition analysis.

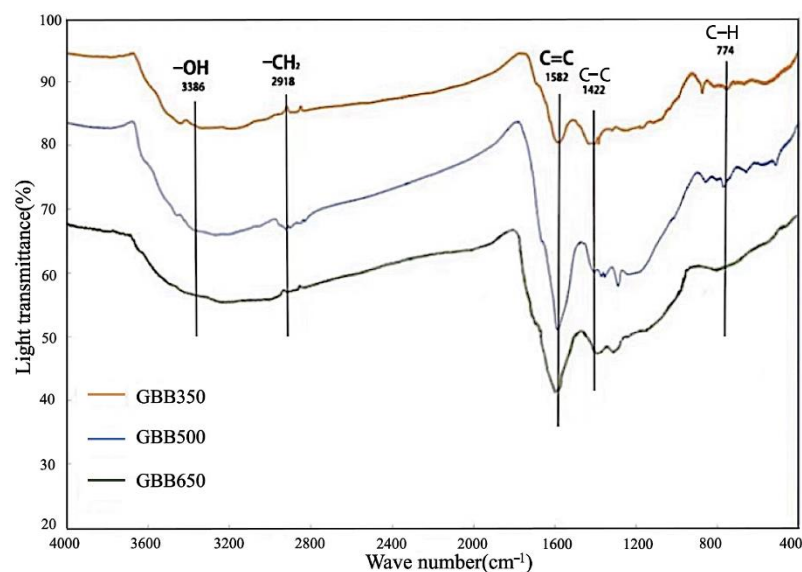


**Figure 4.** Infrared spectrum analysis of GBB at different temperatures.

### 3.5. Brauer–Emmett–Teller (BET) Analysis

The statistics of specific surface area and pore volume of GBB prepared at three temperatures were analyzed above using a fully automatic specific surface area and porosity analyzer to obtain Table 2. It can be seen that as the preparation temperature increases, the high temperature causes the substances contained in the biochar to continuously pyrolyze and produce a large amount of pyrolysis gas volatilization, which makes the biochar produce more pores, and the specific surface area also increases exponentially. The total pore volume of biochar increased gradually from 0.08 m<sup>3</sup>/g to 0.25 m<sup>3</sup>/g with the increase in preparation temperature, the proportion of micropores was increasing, and the distribution of micropore pore size was getting smaller and smaller. The higher the preparation temperature, the greater the number of micropores and the smaller the pore size. The higher the preparation temperature, the greater the number of micropores and the smaller the pore size. The specific surface area of biochar increased significantly from 77.40 m<sup>2</sup>/g to 788.83 m<sup>2</sup>/g with the increase in temperature, which means that the adsorption performance of biochar would be enhanced with the increase in preparation temperature.

**Table 2.** Specific surface area and pore volume of GBB at different preparation temperatures.

Preparation Temperature (°C)	BET Surface Area (m <sup>2</sup> /g)	t-Plot Micropore Area (m <sup>2</sup> /g)	Total Pore Volume (m <sup>3</sup> /g)	t-Plot Micropore Volume (m <sup>3</sup> /g)
300	77.40	90.33	0.08	/
500	310.21	241.38	0.10	0.09
650	788.83	365.86	0.25	0.17

The specific surface area and pore size distribution of the three biochars prepared at 650 °C were determined by nitrogen adsorption–desorption curves. Figure 5a,c,e are the adsorption–desorption curves of GBB650, QBB650, and SBB650, respectively. The adsorption–desorption curves of the three biochars were similar to each other. Taking the adsorption–desorption curve of GBB as an example, the N<sub>2</sub> adsorption amount of GBB rose sharply when the relative pressure rose to 0.02 and became less when the relative pressure was 0.05. After that, the N<sub>2</sub> adsorption amount of GBB increased slowly by increasing the relative pressure value. The observation of the pore size distribution graph shows that it appears similar to the type III isotherm, i.e., no B point appears. This indicates that microporous filling did not occur in the low-pressure region, suggesting that

the biochar formed very few microporous pores and was mainly dominated by narrow fissure mesopores.

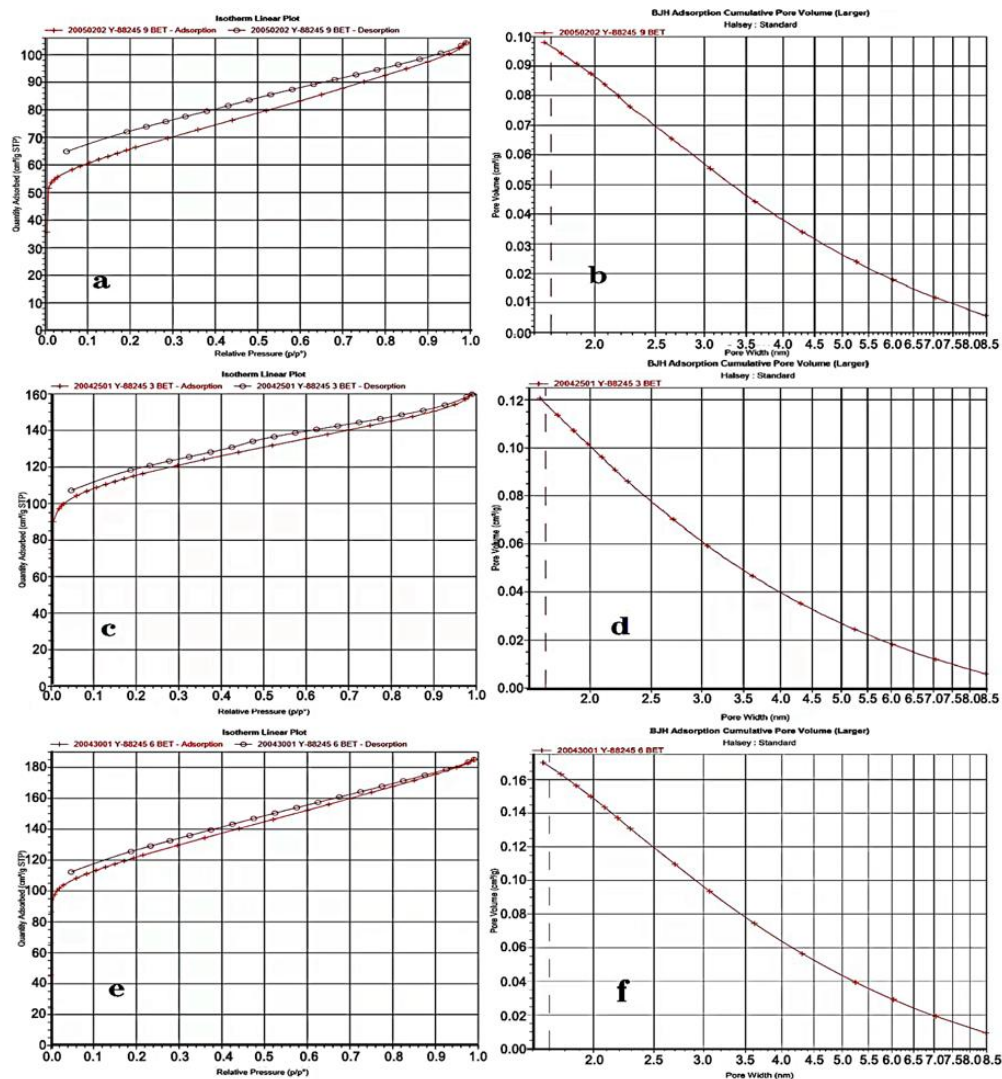


**Figure 5.** N<sub>2</sub> adsorption–desorption of (a) GBB650, (c) QBB650 and (e) SBB650; and pore size distribution of (b) GBB650, (d) QBB650 and (f) SBB650 prepared at preparation temperature T = 650 °C.

For the three biochars, the specific surface area and pore volume of biochars prepared at the same 650 °C are shown in Table 3. The BET-specific surface area of GBB650 is nearly 1.8 times higher than that of the other two biochars, while the micropore-specific surface area is 365.86 m<sup>2</sup>/g, and the total pore volume is 0.25 cm<sup>3</sup>/g, the micropore volume is 0.17 m<sup>3</sup>/g. In comparison with the other two biochars, the microporous specific surface area, total pore volume, and microporous volume of GBB650 were significantly higher than those of QBB650 and SBB650. We can see from the pore size distribution diagram of BJH that the pore sizes of the three biochars prepared at 650 °C were mainly distributed between 2.1 and 5.5 nm. In general, GBB650 formed the most developed pores and had the largest specific surface area, which further explained its stronger adsorption performance as well as the large adsorption capacity.

**Table 3.** Specific surface area and pore volume of three types of biochar prepared at 650 °C.

Biochar Types	BET Surface Area (m <sup>2</sup> /g)	t-Plot Micropore Area (m <sup>2</sup> /g)	Total Pore Volume (m <sup>3</sup> /g)	t-Plot Micropore Volume (m <sup>3</sup> /g)
SBB650	428.83	345.39	0.24	0.15
QBB650	459.19	290.34	0.12	0.08
GBB650	788.83	365.86	0.25	0.17

3.6. Thermogravimetric Analysis

The thermogravimetric analysis graphs of the three biochars prepared at preparation temperature T = 500 °C are shown in Figure 6. The trend of the thermogravimetric change curve of the three biochars is relatively similar; taking GBB500 as an example, it can be concluded from the graph that the trend of the thermogravimetric change curve is divided into three main stages. In the first stage, the weight loss from room temperature to 225 °C is 6.160%, and the loss is mainly due to the decomposition of functional groups on the surface of biochar, and the weight loss rate in this stage is faster. This is mainly because the absorbed water vapor and surface functional groups have been lost, and the mass loss starts to slow down. In this stage, the TG curve started to decline rapidly again. The heat difference curve also kept decreasing, indicating that the sample was losing mass rapidly while absorbing heat continuously. From the DTG curves, it can be seen that in the third stage, GBB500 has the maximum rate of weight loss at 600 °C, SBB500 has the maximum rate of weight loss at 625 °C, and QBB500 has the maximum rate of weight loss at 615 °C. From this, it can be inferred that the charring completion temperature of the three biomasses GBB500 < QBB500 < SBB500. The third stage is 480.55–800 °C, and this stage is mainly the thermal decomposition stage of the biochar, which is the period of rapid loss of this biochar with a mass loss rate of 14.49%, which is probably caused by the aromatization condensation of the biochar under the action of high temperature.

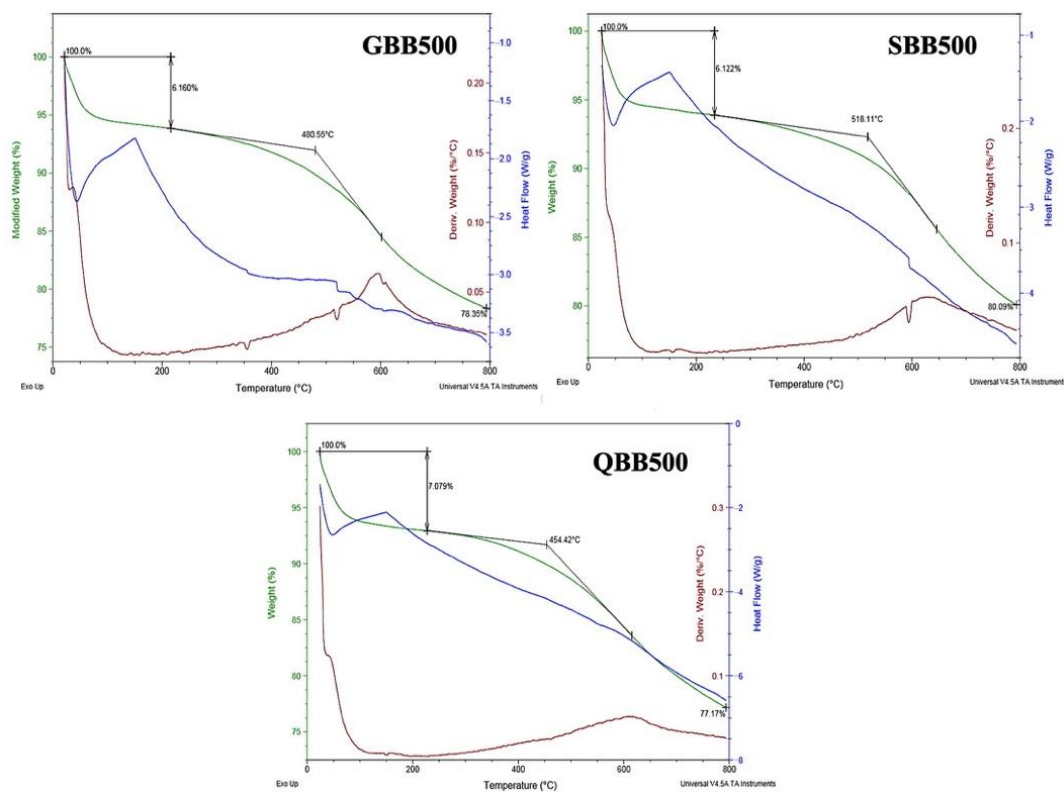


**Figure 6.** Thermogravimetric analysis of three types of biochar prepared at preparation temperature T = 500 °C.

### 3.7. Analysis of RSM

#### 3.7.1. BBD Model

According to the results of the single-factor experiment, this experiment uses Design Expert 8.0.6 software to Design and analyze the scheme of different biological carbon dosages, biological carbon preparation temperature, and experimental temperature mixture experiment. The BBD model was used to design the three-factor and three-level experimental scheme with 17 experimental sites. The coding and level values of experimental factors are shown in Table 4.

**Table 4.** Coding and level values of experimental factors.

Factor	Code	Standard		
		−1	0	+1
dosage (g)	X <sub>1</sub>	0.1	0.3	0.5
temperature (K)	X <sub>2</sub>	298	308	318
Preparation temperature (°C)	X <sub>3</sub>	350	500	650

Tables 4 and 5 show the variance calculation and significance analysis results of the established model. F value is the mean square error of regression/actual error, representing the significance of various factors influencing the model on the response value. The closer the R<sup>2</sup> value is to 1, the higher the fit degree is.  $p < 0.01$  indicated that the influence was highly significant,  $p < 0.05$  indicated that the influence was significant, and  $p > 0.1$  indicated that the influence was insignificant. Adeq Precision refers to the Precision of the model, whose value is greater than 4, indicating high Precision of the model.

**Table 5.** Experimental design and analysis results (taking the preparation of biological carbon by 500 degrees of GBB as an example).

Order Number	Value of Each Factor			Q <sub>Act</sub> (mg/kg)	Q <sub>Pre</sub> (mg/kg)
	X <sub>1</sub> (g/L)	X <sub>2</sub> (K)	X <sub>3</sub> (°C)		
1	0.10	298.00	500	11.76	
2	0.50	298.00	500	3.92	
3	0.10	318.00	500	12.64	
4	0.50	318.00	500	3.97	12.84
5	0.10	308.00	350	12.36	2.83
6	0.50	308.00	350	2.64	13.74
7	0.10	308.00	650	19.48	2.89
8	0.50	308.00	650	3.98	11.65
9	0.30	298.00	350	3.22	4.06
10	0.30	318.00	350	4.24	18.06
11	0.30	298.00	650	6.62	4.74
12	0.30	318.00	650	6.81	2.89
13	0.30	308.00	500	6.53	3.90
14	0.30	308.00	500	6.47	6.93
15	0.30	308.00	500	6.38	6.95
16	0.30	308.00	500	6.33	6.56
17	0.30	308.00	500	6.61	6.56

Expert Design software is used to analyze the experimental data and calculate each parameter, and the model equation is as follows:

$$Y_{R-R} = 6.57 - 5.21X_1 + 0.24X_2 + 1.79X_3 - 0.21X_1X_2 - 1.44X_1X_3 - 0.26X_2X_3 + 2.97X_1^2 - 1.46X_2^2 + 0.081X_3^2 \quad (2)$$

Significance analysis of regression equation for cadmium ion adsorption by three biochar are shown in Table 6. It can be seen that the effect of the three biochar dosing amounts D (X<sub>1</sub>) and biochar preparation temperature T (X<sub>3</sub>) on the adsorption capacity

of Cd<sup>2+</sup> was very significant ( $p < 0.01$ ). However, the experimental temperature value ( $X_2$ ) had little effect on the adsorption capacity of Cd<sup>2+</sup> ( $p > 0.1$ ). The regression equation ANOVA results for the adsorption of cadmium ions by the three biochar species are shown in Table 7. The coefficient of determination  $R^2$  of QBB is 0.9736, with a small experimental error, a high correlation between the measured and predicted values and a good fit with a corrected coefficient of determination  $R_{Adj}^2 = 0.9398$ . Only 6% of the components could not be explained by the model; with an Adeq Precision of 18.366, the precision of the model is very high. The coefficients of determination of GBB and SBB were 0.9662 and 0.9618, respectively, indicating that the experimental error was larger than that of QBB, and the correction coefficient of determination was greater than 0.9, which could explain more than 90% of the response variable, and the Adeq Precision were all close to or greater than 15, with high precision.

**Table 6.** Significance analysis of regression equation for cadmium ion adsorption by three biochar.

GBB			QBB			SBB		
Sources of Variation	F	<i>p</i>	Sources of Variation	F	<i>p</i>	Sources of Variation	F	<i>p</i>
Model	22.29	0.0002	Model	28.41	0.0001	Model	19.61	0.0004
$X_1$	147.0	<0.0001	$X_1$	182.8	<0.0001	$X_1$	132.6	<0.0001
$X_2$	0.319	0.5893	$X_2$	0.10	0.7576	$X_2$	0.147	0.7125
$X_3$	17.26	0.0043	$X_3$	31.62	0.0008	$X_3$	22.30	0.0022
$X_1X_2$	0.115	0.7435	$X_1X_2$	0.115	0.7443	$X_1X_2$	0.285	0.6097
$X_1X_3$	5.64	0.0491	$X_1X_3$	7.46	0.0292	$X_1X_3$	0.243	0.6370
$X_2X_3$	0.18	0.6779	$X_2X_3$	0.021	0.8881	$X_2X_3$	0.028	0.8701
$X_1^2$	25.10	0.0015	$X_1^2$	29.41	0.0010	$X_1^2$	17.91	0.0039
$X_2^2$	6.1	0.0428	$X_2^2$	5.41	0.0529	$X_2^2$	3.73	0.0946
$X_3^2$	0.018	0.8955	$X_3^2$	0.054	0.8214	$X_3^2$	0.007	0.9320
Lack of Fit	90.74	0.0004	Lack of Fit	90.42	0.0004	Lack of Fit	1075.36	<0.0001

**Table 7.** Analysis of variance of the regression equation for cadmium ion adsorption by three bioches.

Variance	GBB	QBB	SBB
$R^2$	0.9662	0.9736	0.9618
$R_{Adj}^2$	0.9229	0.9398	0.9128
Adeq Precision	16.339	18.366	14.973

### 3.7.2. Comparative Study on Adsorption Capacity

The Expert Design software was used to analyze the experimental data, and it was found that the dosage and preparation temperature of the three conditions had the most significant influence on the adsorption capacity of biological carbon. Then, we used the software to obtain the three-dimensional effect of adsorption of the three types of biochar under optimal adsorption conditions, as shown in Figure 7. From the figure, GBB650 can reach a maximum unit adsorption capacity of nearly 20 mg/g at 0.1 g of biochar. The highest unit adsorption of QBB and SBB was 16 mg/g and 12 mg/g, respectively, which showed that the adsorption capacity of GBB was better than QBB and SBB biochar under the same conditions.

### 3.7.3. Analysis of the Interaction of Factors

Three-dimensional analysis was carried out using Design-Expert software, and the response surface and contour lines of GBB were drawn, as shown in Figures 8–10. The interactive influence of various variable factors was analyzed. As can be seen in Figure 8, the interaction between the dosing quantity and preparation temperature between 350 °C to 650 °C is significant; as the biological carbon preparation temperature rise, the biological carbon of cadmium adsorption capacity also gradually increases, and the slope along with the pitch change with the increase of the amount of steep, that the preparation of

the influence of temperature and additive quantity, this is consistent with the variance of the model results. It can be seen from the contour diagram that the interaction between the two is significant. As can be seen from the three-dimensional Figure of Figure 9, the dosage of biological carbon (D) is in the range of 0.1–0.5 g, and the unit equilibrium adsorption capacity decreases with the increase of the dosage. The change in experimental temperature has little influence on the adsorption capacity, which is consistent with the results of the single-factor experiment. Biological carbon can be seen in Figure 10, with no significant interaction between temperature and the experiment temperature, between 298–318 K. As the temperature increases, the biological carbon adsorption capacity of cadmium ions reduces after rising first, and the gradient along the temperature change is not obvious. Explaining the influence of experimental temperature on the adsorption capacity is not obvious. This is consistent with the variance of the model results. It can be seen that among the three conditions affecting the adsorption capacity of biological carbon, including preparation temperature, experimental temperature, and biological carbon dosage, the dosage has the most obvious effect. With the increase in dosage, the amount of heavy metal adsorbed by biological carbon increases, while the amount of biological carbon per unit mass decreases, followed by the preparation temperature of biological carbon, The three kinds of three-dimensional images of biological carbon all reflect that the adsorption capacity of cadmium increases with the increase of biological carbon preparation temperature, but the effect of experimental temperature is not significant from the experimental results.

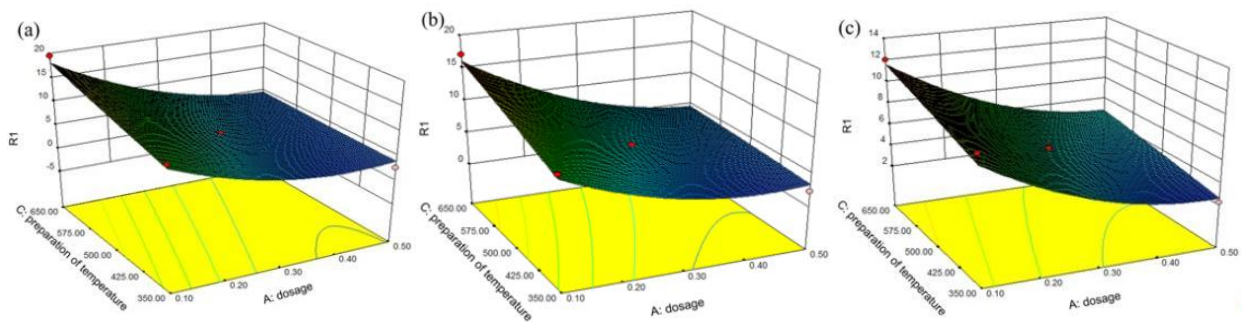


Figure 7. (a) GBB, (b) QBB, (c) SBB biochar adsorption capacity.

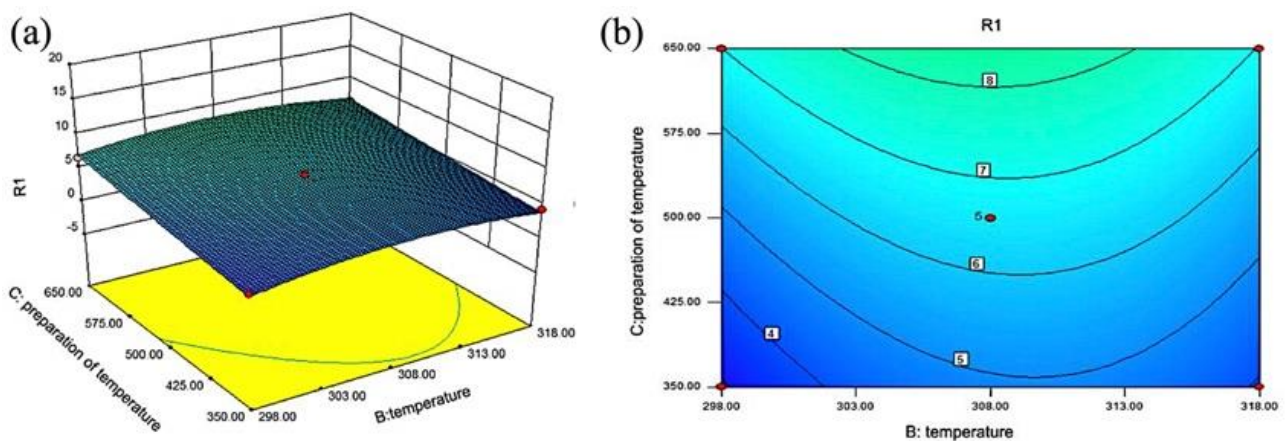


Figure 8. The (a) three-dimensional view and (b) top view for interaction between experimental temperature and preparation temperature T.

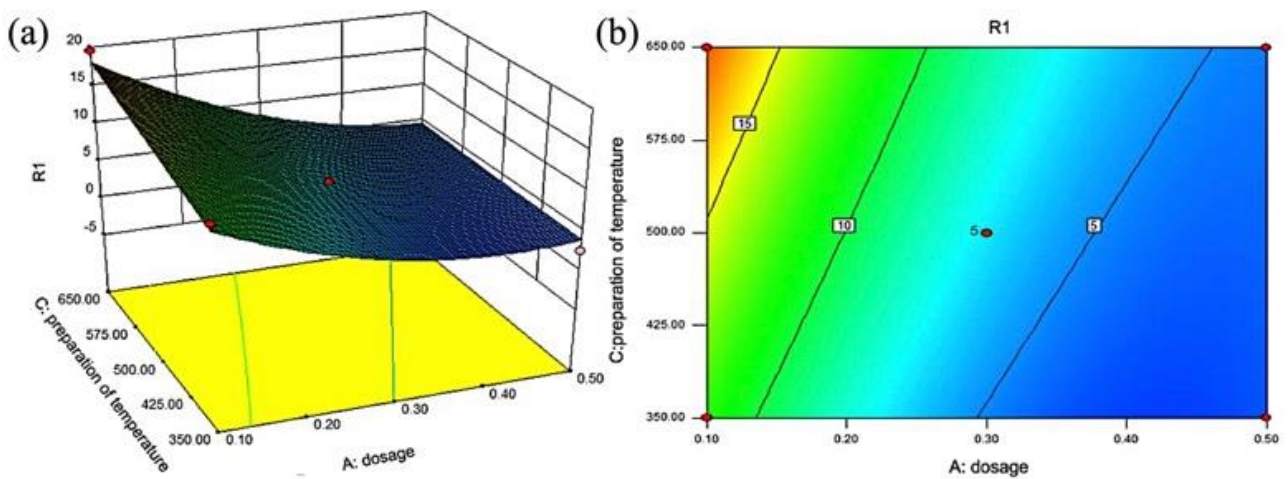


Figure 9. The (a) three-dimensional view and (b) top view for interaction between dosage D and preparation temperature T.

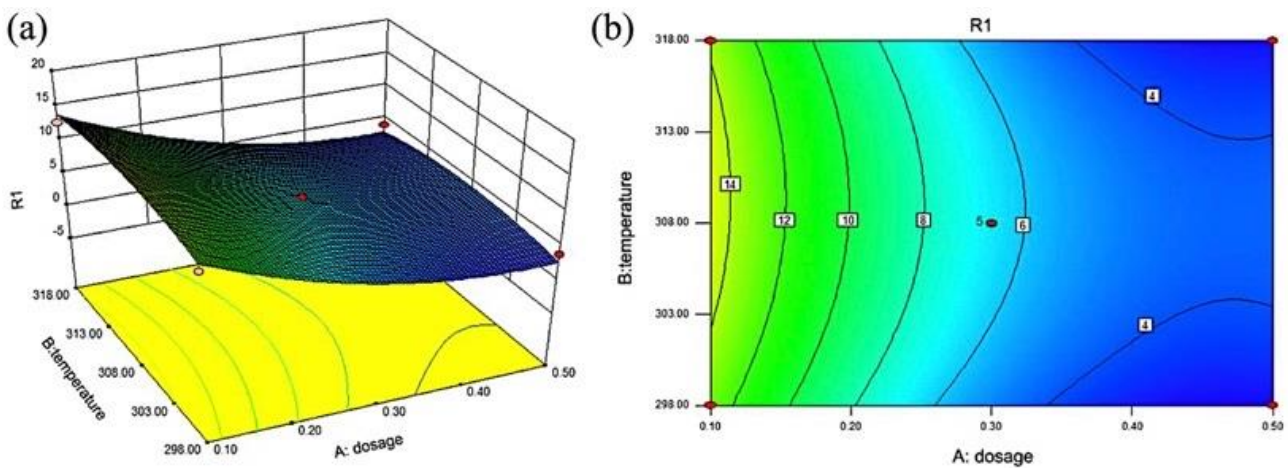


Figure 10. The (a) three-dimensional view and (b) top view for interaction between dosage D and experimental temperature.

#### 4. Conclusions

In summary, among the three factors affecting the adsorption capacity of biochar, the preparation temperature of biochar is the most important factor, followed by the dosage of biochar, and the effect of experimental temperature is relatively weak. Response surface method (RSM) using Box–Behnken Design (BBD) to optimize the preparation factor can maximize the adsorption capacity and removal rate of  $\text{Cd}^{2+}$ . RSM showed that GBB650 was predicted to have the best adsorption capacity of 18.06 mg/g per unit of GBB at an experimental temperature of 25 degrees Celsius with 0.1 g of biochar, which was better than the best adsorption capacity of 16.08 mg/g for QBB and 11.65 mg/g for SBB. The experimental values of  $\text{Cd}^{2+}$  adsorption on the three biochars were 19.48 mg/g, 17.15 mg/g, and 12.04 mg/g. The deviations from the predicted values were 7.86%, 6.8%, and 2.9%, respectively. The results show that the mathematical model of the response surface method can fit the experimental data well and can predict the adsorption results of biochar quickly and accurately compared with the traditional adsorption test. The analysis of BET, pore size distribution, SEM, and FTIR showed that the biochar was mainly used for the adsorption of  $\text{Cd}^{2+}$  through  $\text{Cd}^{2+}$  and ion exchange reaction and functional groups as well as physical adsorption, and the analytical results were consistent with the optimized results of RSM method.

**Author Contributions:** Conceptualization, methodology, writing—original draft, data curation and writing—review & editing W.L.; software, H.K.; formal analysis and investigation, X.W.; visualization, D.Z. All authors have read and agreed to the published version of the manuscript.

**Funding:** This research received no external funding.

**Institutional Review Board Statement:** Not applicable.

**Informed Consent Statement:** Not applicable.

**Data Availability Statement:** The data presented in this study are available upon request from the corresponding author or the first author.

**Conflicts of Interest:** The authors declare no conflict of interest.

## References

1. Feng, L.; Luo, J.; Chen, Y. Dilemma of sewage sludge treatment and disposal in China. *Environ. Sci. Technol.* **2015**, *49*, 4781–4782. [[CrossRef](#)] [[PubMed](#)]
2. Xie, F.; Jin, L.; Tu, J.; Le, M.; Wang, F. Advances in research on comprehensive utilization of tea waste. *Agric. Sci. Technol.* **2015**, *16*, 1552–1557.
3. Brudevold, F.; Reda, A.; Aasenden, R.; Bakhos, Y. Determination of trace elements in surface enamel of human teeth by a new biopsy procedure. *Arch. Oral Biol.* **1975**, *20*, 667–673. [[CrossRef](#)]
4. Guo, W.; Wu, T.; Jiang, G.; Pu, L.; Zhang, J.; Xu, F.; Yu, H.; Xie, X. Spatial Distribution, Environmental Risk and Safe Utilization Zoning of Soil Heavy Metals in Farmland, Subtropical China. *Land* **2021**, *10*, 569. [[CrossRef](#)]
5. Wang, L. Exploration of Strategies for Chronic Disease Prevention and Control and Relevant System Development in China. *Front. Eng. Manag.* **2015**, *2*, 2. [[CrossRef](#)]
6. Wang, Z.Y.; Zhao, J.; Song, L.; Mashayekhi, M.; Chefetz, B.; Xing, B. Adsorption and desorption of phenanthrene on carbon nanotubes in simulated gastrointestinal fluids. *Environ. Sci. Technol.* **2011**, *45*, 6018–6024. [[CrossRef](#)]
7. Deng, G.; Li, M.; Li, H.; Yin, L.; Li, W. Exposure to cadmium causes declines in growth and photosynthesis in the endangered aquatic fern (*Ceratopteris pteridoides*). *Aquat. Bot.* **2014**, *112*, 23–32. [[CrossRef](#)]
8. Sun, X.; Zhang, L.; Zhang, B. Research on the coal industry development and transition in China under the background of carbon neutrality. *China Min. Mag.* **2021**, *30*, 1–6.
9. Xin, H.; Ding, Z.H.; Zimmerman, A.R.; Wang, S.; Gao, B. Batch and column sorption of arsenic onto iron-impregnated biochar synthesized through hydrolysis. *Water Res.* **2015**, *68*, 206–216.
10. Keiluweit, M.; Nico, P.S.; Johnson, M.G.; Kleber, M. Dynamic Molecular Structure of Plant Biomass-Derived Black Carbon (Biochar). *Environ. Sci. Technol.* **2010**, *44*, 1247–1253. [[CrossRef](#)]
11. Chen, S.; Qiu, L.; Cheng, H.-M. Carbon-based fibers for advanced electrochemical energy storage devices. *Chem. Rev.* **2020**, *120*, 2811–2878. [[CrossRef](#)] [[PubMed](#)]
12. Sun, Z.; Fang, S.; Hu, Y.H. 3D graphene materials: From understanding to design and synthesis control. *Chem. Rev.* **2020**, *120*, 10336–10453. [[CrossRef](#)] [[PubMed](#)]
13. Jobby, R.; Jha, P.; Yadav, A.K.; Desai, N. Biosorption and biotransformation of hexavalent chromium [Cr(VI)]: A comprehensive review. *Chemosphere* **2018**, *207*, 255–266. [[CrossRef](#)] [[PubMed](#)]
14. Tan, X.F.; Liu, Y.G.; Zeng, G.M.; Wang, X.; Hu, X.; Gu, Y.; Yang, Z. Application of biochar for the removal of pollutants from aqueous solutions. *Chemosphere* **2015**, *125*, 70–85. [[CrossRef](#)]
15. Balwant, S.; Bhupinderpal, S.; Annetel, C. Characterisation and evaluation of biochars for their application as a soil amendment. *Soil Res.* **2010**, *48*, 516–525.
16. Zhou, J.; Chen, H.; Thring, R.W.; Arocena, J.M. Chemical pretreatment of rice straw biochar: Effect on biochar properties and hexavalent chromium adsorption. *Int. J. Environ. Res.* **2019**, *13*, 91–105. [[CrossRef](#)]
17. Ye, L.; Zhang, J.; Zhao, J.; Luo, Z.; Tu, S.; Yin, Y. Properties of biochar obtained from pyrolysis of bamboo shoot shell. *J. Anal. Appl. Pyrolysis* **2015**, *114*, 172–178. [[CrossRef](#)]
18. Moradi-Choghamarani, F.; Moosavi, A.A.; Sepaskhah, A.R.; Baghernejad, M. Physico-hydraulic properties of sugarcane bagasse-derived biochar: The role of pyrolysis temperature. *Cellulose* **2019**, *26*, 7125–7143. [[CrossRef](#)]
19. Khanmohammadi, Z.; Afyuni, M.; Mosaddeghi, M.R. Effect of pyrolysis temperature on chemical and physical properties of sewage sludge biochar. *Waste Manag. Res.* **2015**, *33*, 275–283. [[CrossRef](#)]
20. Huang, Z.; Wu, X.; Zhao, F.; Lu, P. Phosphorus Adsorption Characteristics of Sediments and Its Influencing Factors in Rongcheng Swan Lake Wetland. *China Water Wastewater* **2009**, *25*, 91–94.
21. Li, Q.; Li, H.; Zhang, S. Yield and water use efficiency of dryland potato in response to plastic film mulching on the Loess Plateau. *Acta Agric. Scand. Sect. B Soil Plant Sci.* **2017**, *68*, 175–188. [[CrossRef](#)]
22. Arias, F.E.A.; Beneduci, A.; Chidichimo, F.; Furia, E.; Straface, S. Study of the adsorption of mercury (II) on lignocellulosic materials under static and dynamic conditions. *Chemosphere* **2017**, *180*, 11–23. [[CrossRef](#)] [[PubMed](#)]

23. Zhao, R.; Li, X.; Sun, B.; Shen, M.; Tan, X.; Ding, Y.; Jiang, Z.; Wang, C. Preparation of phosphorylated polyacrylonitrile-based nanofiber mat and its application for heavy metal ion removal. *Chem. Eng. J.* **2015**, *268*, 290–299. [[CrossRef](#)]
24. Septiana, L.M.; Djajakirana, G.; Darmawan, D. Characteristics of Biochars from Plant Biomass Wastes at Low-Temperature Pyrolysis. *SAINS TANAH J. Soil Sci. Agroclimatol.* **2018**, *15*, 15–28. [[CrossRef](#)]
25. Li, H.; Mahyoub, S.A.A.; Liao, W.; Xia, S.; Zhao, H.; Guo, M.; Ma, P. Effect of pyrolysis temperature on characteristics and aromatic contaminants adsorption behavior of magnetic biochar derived from pyrolysis oil distillation residue. *Bioresour. Technol.* **2017**, *223*, 20–26. [[CrossRef](#)]
26. Ahmad, M.; Rajapaksha, A.U.; Lim, J.E.; Zhang, M.; Bolan, N.; Mohan, D.; Vithanage, M.; Lee, S.S.; Ok, Y.S. Biochar as a sorbent for contaminant management in soil and water: A review. *Chemosphere* **2014**, *99*, 19–33. [[CrossRef](#)]
27. Liu, K.; Bai, Y.; Kang, Y.X.; Zhang, L. Investigation of particle characteristics, composition, and microstructure of LaxCe1 (-) O-x(2) (-) (x/2) thermal barrier coatings during supersonic atmospheric plasma spray using Box-Behnken design. *Surf. Coat. Technol.* **2016**, *286*, 9–15. [[CrossRef](#)]
28. Nisar, S.; Hanif, M.A.; Zahid, M.; Ghaffar, A. Enzymatic glycosylation of menthol: Optimization of synthesis and extraction processes using response surface methodology and biological evaluation of synthesized product. *Chem. Pap.* **2022**, *76*, 2649–2675. [[CrossRef](#)]
29. Lakshmi, E.S.; Rao, M.R.N.; Sudhamani, M. Response surface methodology-artificial neural network-based optimization and strain improvement of cellulase production by *Streptomyces* sp. *Biosci. J.* **2020**, *36*, 1390–1402.
30. Yao, T.; Guo, S.; Zeng, C.; Wang, C.; Zhang, L. Investigation on efficient adsorption of cationic dyes on porous magnetic polyacrylamide microspheres. *J. Hazard. Mater.* **2015**, *292*, 90–97. [[CrossRef](#)]
31. Liu, W.; Li, W.; Jiang, H.; Yu, H.Q. Fates of Chemical Elements in Biomass during Its Pyrolysis. *Chem. Rev.* **2017**, *117*, 6. [[CrossRef](#)] [[PubMed](#)]